Chemical and Biological Technologies in Agriculture

RESEARCH

Open Access

Antivirus isoindolinone alkaloids with rare oxocyclopenta[*f*]isoindole frameworks isolated from the stems of flue cured tobacco

Qiu-Fen Hu[1,2], Yue-Yu Ma[1], Hua-Yin Liu[1,2], Jia-Meng Dai[2], Feng-Xian Yang[2], Jian-Duo Zhang[2], Jin Wang[2], Xue-Mei Li[2], Xin Liu[2], Jing Li[2], Yin-Ke Li[1,2], Wei-Guang Wang[1], Min Zhou[1*] and Guang-Yu Yang[2*]

Abstract

Background: Since *Nicotiana tabacum* (tobacco) has important significance to humans for their medicinal uses, to find antivirus activities inhibitors from tobacco, increase its medicinal value, and comprehensive utilization of its by-products, our group had investigated the chemical constituents of the stems of Y-202, a cultivar of tobacco which high resistance to tobacco mosaic virus (TMV).

Results: Four new isoindolinone-type alkaloids, nicoisoindoles A–D (**1**–**4**), along with four known isoindole derivatives (**5**–**8**) were isolated. Compounds **1**–**4** represent a new subclass of isoindolinone alkaloids with rare cyclopenta[*f*] isoindole-1-one frameworks. Among them, nicoisoindole C (**3**) possesses an unusual *N*-2-(5-methoxy-6-methylpyridin-2-yl) ethyl moiety, while nicoisoindole D (**4**) has a novel a *N*-(3-methyl-6-oxo-1,6-dihydropyridin-2-yl)methyl substituent. Interestingly, compounds **1**, **3,** and **4** showed high anti-TMV activities with inhibition rates of 43.8%, 58.8%, and 67.8% at the concentration of 20 μM, and IC_{50} values of 23.6, 19.5 and 15.4 μM, respectively, even more potent than that of positive control.

Conclusions: The successful isolation and structure identification of new oxocyclopenta[*f*]isoindole-1-ones provide materials for the screening of antivirus activities inhibitors, and contribute to the development and utilization of the waste from tobacco cultivation.

Keywords: *Nicotiana tabacum*, Nicoisoindoles A–D, Isoindolinone alkaloids, Rare cyclopenta[*f*]isoindole-1-one frameworks, Antivirus activities, molecular docking

*Correspondence: zhouminynun@163.com; ygy1110@163.com

[1] Key Laboratory of Natural Products Synthetic Biology of Ethnic Medicinal Endophytes, State Ethnic Affairs Commission, Yunnan Minzu University, Kunming 650031, People's Republic of China
[2] Yunnan Key Laboratory of Tobacco Chemistry, China Tobacco Yunnan Industrial Co., Ltd, Kunming 650231, People's Republic of China

Graphical Abstract

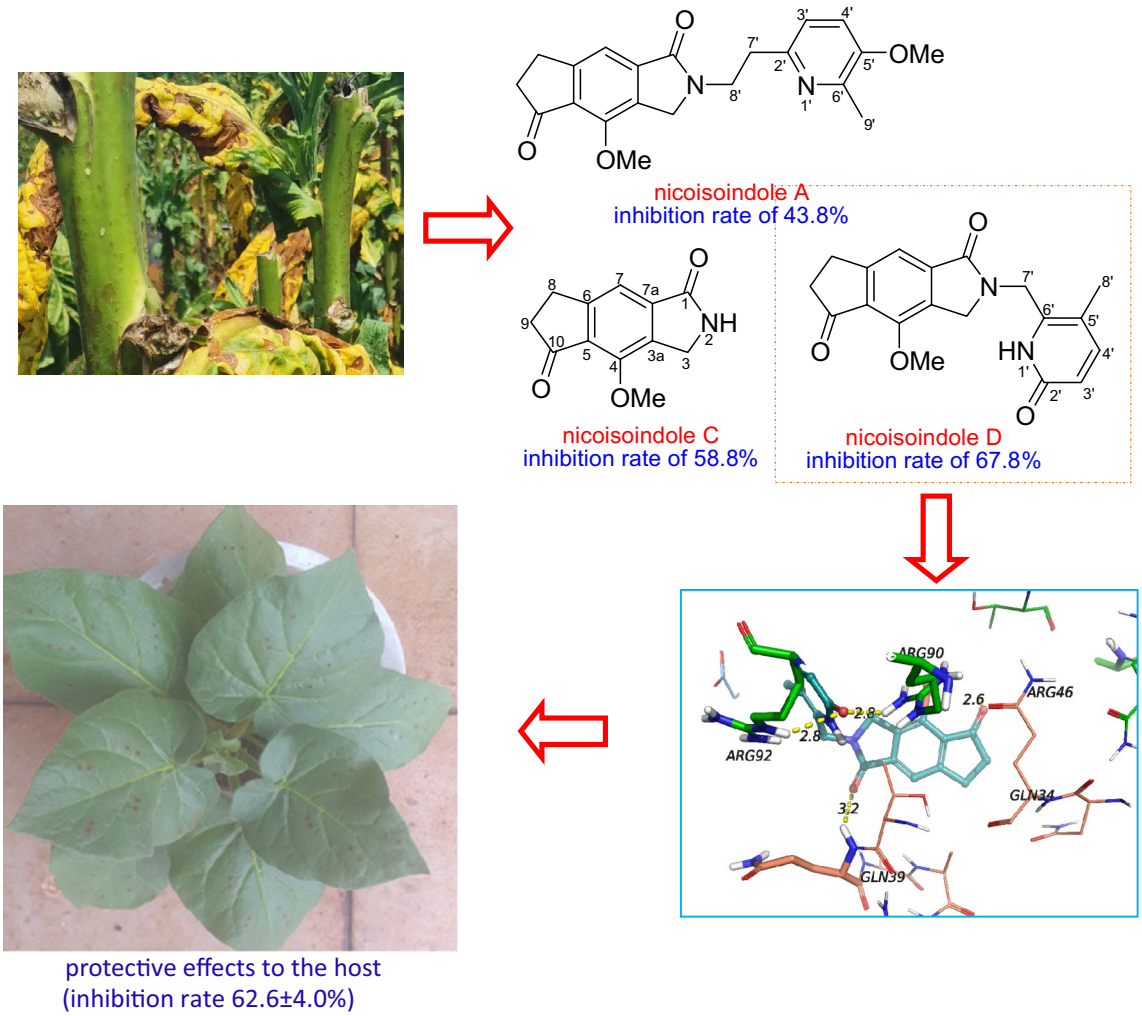

Background

Tobacco (*Nicotiana tabacum* L.) is a plant of the genus *Nicotiana* (Solanaceae family), whose leaves are widely used for smoking, chewing, and isolation of nicotine, ordinarily after processing by a series of ways [1]. In addition, tobacco also has important significance to humans for their ornamental values and medicinal uses [2]. In recent years, many bioactive naturally small molecule metabolites have been reported from this genus, including diterpenoids [3], sesquiterpenoids [4, 5], flavonoids [6, 7], coumarins [8, 9], furans [10, 11], alkaloids [12, 13], sterols [6], and the like. The biosynthesis and pharmacological properties of some metabolites also have been widely elucidated, such as pyridine alkaloids, including the eponymous nicotine [14], isoprenoids [15], aromatic compounds [16], and polyphenols [17].

Flue-cured tobacco, a variety of *N. tabacum*, is a major cash crop in Yunnan province, P.R. China. Yunnan province produces approximately 750,000 tons of flue-cured tobacco on 32 0,000 hectares of land every year, accounting for about 50% of the country's total tobacco production [18]. The large-scale tobacco planting produces a large amount of waste, including stem, roots, low grade and defective tobacco leaves. Therefore, the multipurpose utilization of the by-product is an interesting topic and arouses more and more attentions [8–10, 19, 20]. To increase the pharmacodynamic value of tobacco, and the comprehensive utilization of its by-products, our group has investigated the chemical constituents of the stems

Table 1 ^{1}H and ^{13}C NMR Data of compounds **1** and **2** (δ in ppm, data obtained in $CDCl_3$)

No	1		2	
	δ_C	δ_H (*J* in Hz)	δ_C	δ_H (*J* in Hz)
1	169.5 (C)		167.5 (C)	
2-NH		9.07, s		
3	43.7 (CH_2)	4.32, s	45.9 (CH_2)	4.16, s
4	156.3 (CH_2)		156.9 (C)	
5	125.1 (C)		123.8 (C)	
6	152.7 (C)		152.4 (C)	
7	116.3 (CH)	7.49, s	115.8 (CH)	7.47, s
3a	128.4 (C)		125.2 (C)	
7a	134.4 (C)		136.8 (C)	
8	28.3 (CH_2)	2.76, t (5.6)	28.1 (CH_2)	2.75, t (5.6)
9	37.2 (CH_2)	3.33, t (5.6)	37.2 (CH_2)	3.35, t (5.6)
10	206.3 (C)		206.4 (C)	
1′			34.2 (CH_3)	2.84, s
-OMe	60.3 (CH_3)	3.83, s	60.4 (CH_3)	3.83, s

Table 2 ^{1}H and ^{13}C NMR Data of compounds **3** and **4** (δ in ppm, data obtained in $CDCl_3$)

No	3		4	
	δ_C	δ_H (*J* in Hz)	δ_C	δ_H (*J* in Hz)
1	167.5 (C)		166.3 (C)	
3	44.2 (CH_2)	4.24, s	39.7 (CH_2)	4.21, s
4	156.8 (C)		156.8 (C)	
5	123.9 (C)		123.7 (C)	
6	152.2 (C)		152.4 (C)	
7	115.7 (CH)	7.48, s	115.4 (CH)	7.50, s
3a	125.1 (C)		125.4 (C)	
7a	136.7 (C)		136.8 (C)	
8	28.2 (CH_2)	2.68, t (5.6)	28.2 (CH_2)	2.68, t (5.6)
9	37.4 (CH_2)	3.36, t (5.6)	37.2 (CH_2)	3.36, t (5.6)
10	206.3 (C)		206.3 (C)	
4-OMe	60.9 (CH_3)	3.82, s	60.9 (CH_3)	3.84, s
2′	153.2 (C)		161.7 (C)	
3′	121.6 (CH)	6.94, d (7.8)	114.6 (CH)	6.74, d (8.8)
4′	122.4 (CH)	7.04, d (7.8)	144.6 (CH)	7.59, d (8.8)
5′	154.4 (C)		118.2 (C)	
6′	145.9 (C)		155.6 (C)	
7′	32.1 (CH_2)	3.16, t (6.2)	52.3 (CH_2)	4.02, s
8′	46.8 (CH_2)	3.56, t (6.2)	14.2 (CH_3)	2.21, s
9′	18.3 (CH_3)	2.32, s		
5′-OMe	55.9 (CH_3)	3.80, s		
1′-NH				8.90, s

of Y-202, a high resistance tobacco mosaic virus (TMV) cultivar of tobacco, which originated from K326 by EMS mutagenesis. As a result, four new isoindolinone-type alkaloids (**1**–**4**) possessing novel cyclopenta[*f*] isoindole-1-one frameworks together with four known analogues (**5**–**8**) were isolated from the title plant. Compounds **1**–**4** were tested for their anti-TMV activities, and their structure–activity relationships were preliminarily verified by molecular docking. The mechanisms study on compound **4** (with the highest anti-TMV activity) was also revealed that the increased potentiation of defense-related enzyme activities, and down-regulate the expression of the NtHsp70 protein may induce resistance in tobacco against the viral pathogen of TMV. Furthermore, to study whether the new compounds have more broad antiviral activities, compounds **1**–**4** were also tested for their anti-rotavirus activities.

Methods

General experimental procedures

IR spectra were obtained using a FTS185 spectrophotometer (Bio-Rad, California, USA). A Shimadzu UV-1900 spectrophotometer (Shimadzu, Kyoto, Japan) was used for scanning UV spectra. The 1D and 2D NMR spectroscopic data were measured by a Bruker DRX-500 NMR spectrometer (Bruker, Karlsruhe, Germany) with TMS as internal standard. Mass spectra were recorded on an Agilent 1290 UPLC with a 6540 Q-TOF mass spectrometer (Agilent Technologies, Wilmington, DE, USA). Semi-preparative HPLC was performed with an Agilent 1260 preparative liquid chromatography (Agilent Technologies, Wilmington, DE, USA) with a Venusil MP C_{18} column (10 μm, 2.0 cm × 25 cm, Agilent, Palo Alto, USA) or a Zorbax PrepHT GF C_{18} column (10 μm, 2.12 cm × 25 cm, Bonna-Agela, Tianjin, China). Column chromatography was performed on silica gel (80–100 mesh or 200–300 mesh) (Qingdao Marine Chemical, Inc., Qingdao, China) and MCI gel (75–150 μm) (Mitsubishi Chemical Corporation, Tokyo, Japan). Fractions were monitored by thin-layer chromatography (Qingdao Marine Chemical, Inc., Qingdao, China) and spots were visualized by heating silica gel plates (approximately 120 °C) sprayed with 5% H_2SO_4 in ethanol.

Plant material

The flue-cured tobacco Y-202, a cultivar with high resistance to TMV, which originated from K326 by EMS mutagenesis was used as plant material. The tobacco was planted in Yuxi area, Yunnan Province. After the tobacco leaves had been harvested, the tobacco stems were collected, and the sample was dried at 35–40 °C, and then crushed with 30–60 mesh. The crushed sample was used for extraction and isolation. The voucher specimen of the

title plant (No. Ynni-19-09-122) has been deposited in School of Ethnic Medicine, Yunnan Minzu University.

Extraction and isolation

The dried stems of *Nicotiana tabacum* (approximately 8.2 kg) were extracted with 70% aqueous acetone, and the total extract was successively partitioned between 3% aqueous tartaric acid and ethyl acetate. Then, the aqueous layer was adjusted to pH 9 by the addition of a saturated aqueous Na_2CO_3solution, which was further extracted with ethyl acetate again. The ethyl acetate residues (146 g) were performed on silica gel (200 mesh, Qingdao Marine Chemical, Inc., Qingdao, China), eluted with trichloromethane/methanol gradient system (10:0, 9:1, 8:2, 7:3, 6:4, and 5:5) to obtain six fractions A–F. Fraction A (9:1, 22.6 g) was separated by silica gel, eluting with trichloromethane/acetone (9:1 to 2:1), yielded subfractions B1–B7. Subfraction B1 (9:1, 3.85 g) was further subjected to silica gel, and then semi-preparative HPLC (58–65% methanol/water, 12 mL/min) to yield **3** (18.5 mg), **4** (19.2 mg), **6** (22.8 mg), **7** (25.4 mg) and **8** (22.6 mg). Subfraction B2 (8:2, 3.21 g) was separated by silica gel and subsequently separated by semi-preparative HPLC (50–55% methanol/water, 12 mL/min) to give **2** (20.5 mg). Subsequently fraction B4 (6:4, 4.15 g) was purified by silica gel and followed by semi-preparative HPL (30–38% methanol/water, 12 mL/min) to yield **1** (26.5 mg) and **5** (23.4 mg).

Nicoisoindole A (**1**): obtained as yellow gum; UV (methanol) λ_{max} nm (log ε) 210 (4.42), 268 (4.15), and 312 (3.58); IR (KBr) ν_{max} 3385, 3142, 2928, 2846, 1686, 1662, 1608, 1582, 1464, 1380, 1268, 1153, 1062, and 825 cm^{-1}; ^1H (500 MHz, $CDCl_3$) and ^{13}C NMR data (125 MHz, $CDCl_3$) see Table 1 and Additional file 1: Figs. S1–S4; positive ESIMS *m/z* 240 $[M+Na]^+$ and positive ESI-HRMS (Additional file 1: Fig. S5) *m/z* 240.0642 $[M+Na]^+$ (calcd. for $C_{12}H_{11}NNaO_3$, 240.0637).

Nicoisoindole B (**2**): obtained as yellow gum; UV (methanol) λ_{max} nm (log ε) 210 (4.46), 266 (4.09), and 310 (3.62); IR (KBr) ν_{max} 3150, 2932, 2839, 1682, 1658, 1612, 1579, 1462, 1383, 1264, 1156, 1068, and 836 cm^{-1}; ^1H (500 MHz, $CDCl_3$) and ^{13}C NMR data (125 MHz, $CDCl_3$) see Table 1 and Additional file 1: Figs. S6–S9; positive ESIMS *m/z* 254 $[M+Na]^+$ and positive ESI-HRMS (Additional file 1: Fig. S10) *m/z* 254.0786 $[M+Na]^+$ (calcd. for $C_{13}H_{13}NNaO_3$, 254.0793).

Nicoisoindole C (**3**): obtained as yellow gum; UV (methanol) λ_{max} nm (log ε) 210 (4.44), 262 (4.15), 287 (3.83), and 316 (3.64); IR (KBr) ν_{max} 3178, 2927, 2846, 1685, 1654, 1615, 1582, 1479, 1380, 1257, 1162, 1068, and 825 cm^{-1}; ^1H (500 MHz, $CDCl_3$) and ^{13}C NMR data (125 MHz, $CDCl_3$) see Table 2 and Additional file 1: Figs. S11–S14; positive ESIMS *m/z* 389 $[M+Na]^+$ and positive ESI-HRMS (Additional file 1: Fig. S15) *m/z* 389.1472 $[M+Na]^+$ (calcd. for $C_{21}H_{22}N_2NaO_4$, 389.1477).

Nicoisoindole D (**4**): obtained as yellow gum; UV (methanol) λ_{max} nm (log ε) 210 (4.52), 268 (4.18), 296 (3.92), and 324 (3.68); IR (KBr) ν_{max} 3368, 3167, 2962, 2938, 2870, 1712, 1683, 1652, 1612, 1567, 1465, 1384, 1276, 1180, 1046, and 863 cm^{-1}; ^1H (500 MHz, $CDCl_3$) and ^{13}C NMR data (125 MHz, $CDCl_3$) see Table 2 and Additional file 1: Figs. S16–S19; positive ESIMS *m/z* 361 $[M+Na]^+$ and positive ESI-HRMS (Additional file 1: Fig. S20) *m/z* 361.1169 $[M+Na]^+$ (calcd. for $C_{19}H_{18}N_2NaO_4$, 361.1164).

Anti-TMV assays

The anti-TMV activities were tested using the half-leaf method [21, 22], and 20 μM of Ningnanmycin ($C_{16}H_{23}O_8N_7$, CAS No. 156410-09-2, Kemike Biomedical Technology Co., Ltd, Wuhan, China), a commercial cytosine nucleoside peptide type antibiotics for plant disease in China) in DMSO was used as a positive control. The virus was inhibited by mixing with the solution of tested compounds (20 μM in DMSO). After 30 min, the mixture was inoculated on the left side of the leaves of *N. glutinosa*, whereas the right side of the leaves was inoculated with the mixture of DMSO solution and the virus as control. The local lesion numbers were recorded 3–4 days after inoculation. Three repetitions were conducted for each compound. The inhibition rates were calculated according to the formula:

$$\text{inhibition rate}\,(\%) = [(C - T)/C] \times 100\%$$

where C is the average number of local lesions of the control and T is the average number of local lesions of the treatment.

For compounds with significant activities in half-leaf method assay, their protective effects on TMV were also evaluated by the pretreating the tobacco plant with 20 μM solutions of compounds or a solution of DMSO for 6 h before inoculation with TMV.

SDS–PAGE and western blot analysis of TMV-CP and Hsp70 protein

The SDS–PAGE was performed as described previously [23], and all reagents were provided by Solarbio science&technology Co., ltd, Beijing, China. Briefly, the tobacco leaves (0.1 g) were ground in the protein loading buffer (40 g/L SDS, 10 mL/L β-ME, 200 mL/L glycerin, 2 g/L bromophenol blue, 0.1 mol/L Tris–HCl, pH 6.8). After centrifuging the lysates, the supernatants were quantitated, dissolved with 5 ×sample loading buffer, and boiled for 7 min. Protein extracts were

subjected to SDS PAGE and transferred to PVDF membranes (Millipore, St. Louis, USA). Membranes were blocked with 5% nonfat milk and incubated overnight with the primary antibodies (of TMV, Hsp70, and β-actin) at 4 °C and then incubated for 1 h at room temperature with fluorescent-labeled secondary antibodies (anti-rabbit IgG) conjugated to horseradish peroxidase. The membranes were then incubated with pierce ECL substrate (Thermo Scientific) and proteins of interest were visualized by chemiluminescent detection on an Image Quant LAS 4000 mini (GE Healthcare).

RT-PCR analysis of TMV-CP

RT-PCR analysis was performed according to previous literature [23], and all reagents were provided by Solarbio science&technology Co., ltd, Beijing, China. Total RNA was extracted from tobacco leaves (0.3 g, fresh weight) using the RNA Easy kit (TianGen, Co. Ltd., Beijing, China) according to the manufacturer's instructions. The purified RNA was reverse transcribed using oligo (dT) primers and Super Script III Reverse Transcriptase (Invitrogen) according to the manufacturer's instructions. The primer sequences were as follows: forward: 5′-GTTGATGAGTTCATGGAAGATG-3′ and reverse: 5′-CAACCCTTC GATTTAAGTGGAG-3′; RdcS forward: 5′ -CCTCTGCAGTTGCCACC-3′ and reverse: 5′-CCTGTGGGTATGCCTTCTTC-3′.

Analysis of defense enzymes activities

After sprayed *N. tabacum* cv. HD plants (a tobacco variety widely cultivated in China) with 20 μM of the compounds, tobacco leaves were harvested on 1, 3, 5, and 7 day post-spraying and used for the determination of the activities of phenylalanine ammonia lyase (PAL), peroxidase (POD), polyphenol oxidase (PPO), and superoxide dismutase (SOD). Activities of PAL, POD, PPO, and SOD were determined using enzyme assay reagent kits following the manufacturer's instructions (Jiancheng Bioengineering Research Institute, Nanjing, China).

Molecular docking

In the current study, molecular docking calculations were executed using AutoDock Vina software. Get 3D TMV-Hel crystal structure from PDB database (PDB: 2OM3), the structures of compounds **1**–**4** were generated by chem3D and the ligands in the crystal structure were split and used as control compound [33]. For molecular docking calculations, the pdbqt files for the proteins and ligands were prepared according to

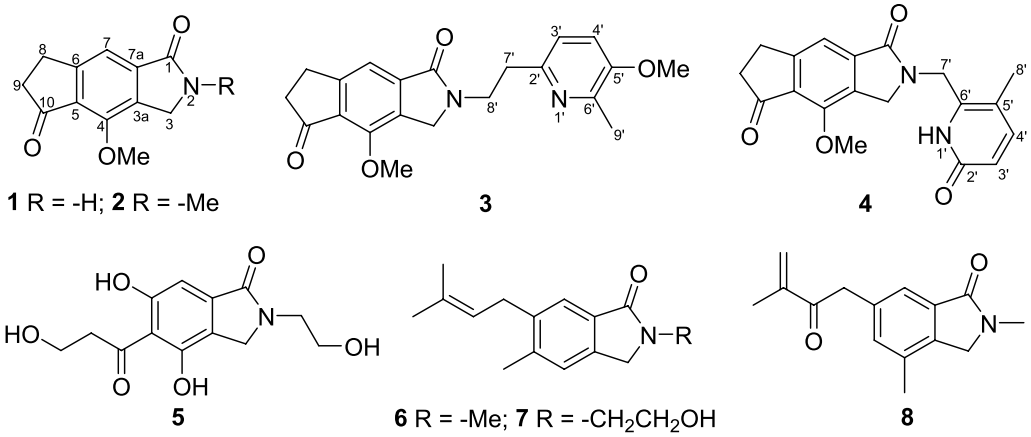

Fig. 1 Isoindolin-1-ones from the flue-cured tobacco

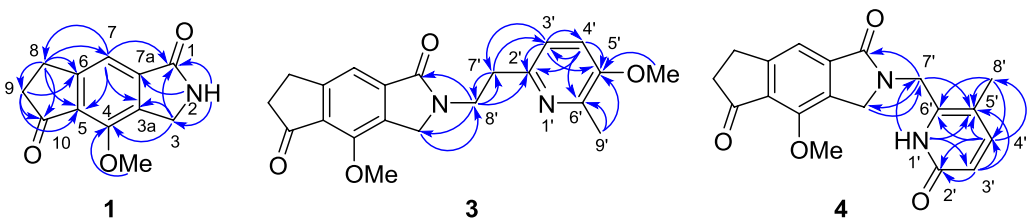

Fig. 2 Key HMBC correlations (H→C) of compounds **1**, **3** and **4**

the AutoDock protocol. All docking parameters were conserved to their default values, except the maximum number of energy evaluation (eval) and the number of genetic algorithms (GA) runs. The docking grid was made to binding site (1.99, − 45.08, 10.25) for the receptor with a grid size of 80 Å* 80 Å *80 Å. The grid spacing value was adjusted to 0.375 Å. Gasteiger atomic partial charges were assigned for all investigated ligands. Molecule interaction were analysis by pymol2.2.

Anti-rotavirus bioassay

The human rotavirus Wa group (obtained from Institute of Medical Biology, Chinese Academy of Medical Sciences, Kunming, China) was used to infect the cell culture MA104 in vitro, the 50% cytotoxicity concentration (CC_{50}) and half maximal effective concentration (EC_{50}) were evaluated, and the ribavirin was used as positive control [24]. MA-104 cells (1×10^5 cells *per* well) were grown in 96-well plates for 48 h. The media were removed and replaced by new media containing serial dilutions of compounds under test. After incubation for 72 h, the media were discarded, and 5.0 μL of MTT solution was added to each well. Plates were then incubated at 37 °C for 4 h. The solution was removed, and 100 μL of 0.04 mol/L HCl-isopropanol were added to each well to dissolve formazan crystals. Using a microplate reader, the absorbance of each well was measured at 540 nm. After subtracting the background absorbance at 655 nm, the 50% CC_{50} of each compound was estimated by regression analysis.

In the mixed treatment assay, each compound was mixed with a 0.01 multiplicity of infection (MOI) of the rotaviruses at various concentrations (1–160 μg/mL) and incubated at 4 °C for 1 h. The mixtures were inoculated in triplicates onto near confluent MA-104 cell monolayers (1×10^5 cells per well) for 1 h with occasional rocking. The solution was removed and the cells replaced with eagles minimum essential medium (EMEM) containing 1 μg/mL trypsin. The cells were incubated for 72 h at 37 °C under 5% CO2 atmosphere until the cells in the control showed complete viral cytopathic effect (CPE) by light microscopy. EC_{50} was estimated by regression analysis.

Results and discussion

Structure characterization of compounds 1–8

The extract prepared from the stems of tobacco was repeatedly separated by various column chromatography and preparative HPLC to afford four new isoindolin-1-ones, nicoisoindoles A–D (**1**–**4**), along with four known isoindole derivatives (**5**–**8**). The structures of the compounds **1**–**8** are shown in Fig. 1, and the ^{1}H and ^{13}C NMR data of **1**–**4** are listed in Tables 1 and 2. The known compounds were identified as 4,6-dihydroxy-2-(2-hydroxyethyl)-5-(3-hydroxypropan)-isoindolin-1-one (**5**) [25], 2,5-dimethyl-6-prenyl-isoindolin-1-one (**6**) [13], 2-(2-hydroxyethyl)-5-methyl-6-prenyl-isoindolin-1-one (**7**) [13], and 2,4-dimethyl-6-(3-methyl-2-oxobut-3-enyl)-isoindolin-1-one (**8**) [12], respectively, by comparison of their NMR data with those reported in the literature.

Compound **1**, a pale-yellow gum, has a molecular formula of $C_{12}H_{11}NO_3$ as revealed from HRMS (ESI) (*m/z* 240.0642 $[M+Na]^+$), suggesting 8 degrees of unsaturation. The IR spectrum showed absorption bands for amine (3385 cm^{-1}), carbonyls (1686 and 1662 cm^{-1}), and aromatic ring (1608, 1582, and 1464 cm^{-1}), and the UV spectrum showed absorption maxima at 268 and 312 nm also suggested the existed of aromatic ring. Its 1D NMR data (Table 1) displayed resonances for 12 carbons and 11 hydrogen atoms, which were ascribed to a 1,2,3,4,5-pentasubstituted benzene ring (C-4 ~ C-6, C-3a, C-7a, H-7), a $-CH_2CH_2CO-$ moiety (C-8 ~ C-10, H_2-8, H_2-9) [26], a amide carbonyl (C-1), an *N*-methylene (C-3 and H_2-3), and a methoxy group (δ_C 60.3 q, δ_H 3.83 s). In addition, the existence of -CH_2CH_2CO- moiety was supported by

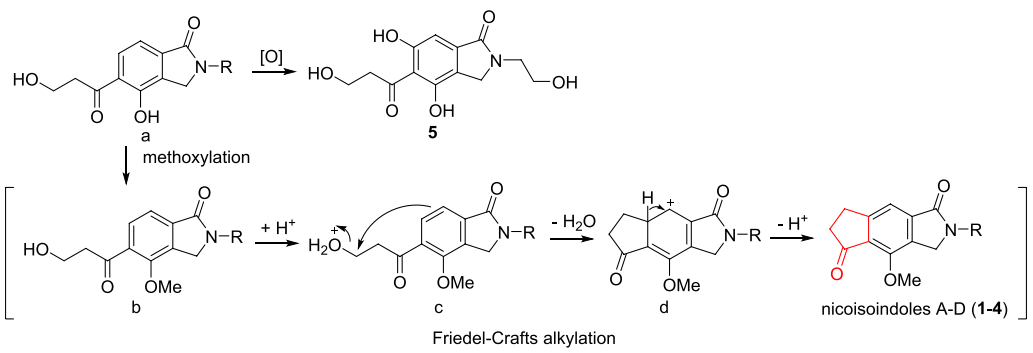

Fig. 3 Plausible biosynthetic pathway of the oxocyclopentane moieties in nicoisoindoles A–D (**1**–**4**)

the HMBC correlations (Fig. 2) from H_2-8 to C-9 and C-10, and from H_2-9 to C-8 and C-10. On the basis of the carbon chemical shifts of these resonances, benzene ring and two carbonyls in compound **1** was accounted for 6 of the 8 degrees of unsaturation. There still two rings should also be existed in compound **1** to meet 8 degrees of unsaturation. By comparison with the published literature, the benzene ring, *N*-methylene, and amide carbonyl should be formed a isoindolin-1-one nucleus [12, 13], while the $-CH_2CH_2CO-$ moiety also should be linked to benzene ring to form a pentacyclic ketone [26, 27]. In addition, the existance of isoindolin-1-one nucleus was supported by the HMBC correlations from H_2-3 to C-1, C-4, C-3a, and C-7a, and from H-7 to C-1, while C-8 linked to C-6, C-10 linked to C-5 to form pentacyclic ketone moiety was also supported by the HMBC correlations from H_2-8 to C-5/C-6/C-7, and from H_2-9 to C-5/C-6 (Fig. 2). Finally, the remained methoxy group substituted at the C-4 was supported by the HMBC correlations from methoxy proton (δ_H 3.83 s) to C-4. Hence, the structure of **1** was assigned, and gave the trivial name of nicoisoindole A.

Nicoisoindole B (**2**) has a molecular formula as $C_{13}H_{13}NO_3$, on the basis of the quasi-molecular ion at *m/z* 254.0786 ($[M+Na]^+$) in the HRMS (ESI). The IR spectrum showed absorption bands for carbonyls (1682 and 1658 cm^{-1}), and aromatic ring (1612, 1579, and 1462 cm^{-1}), and the UV spectrum showed absorption maxima at 266 and 310 nm also suggested the existed of long conjugated system. The 1D NMR, spectra of **2** were very similar to those of **1**. The chemical shift differences were the appearance of an additional *N*-methyl group, and the disappearance of amino hydrogen group in **2**. In addition, *N*-2 proton replaced by methyl group was also confirmed by the HMBC correlations from the *N*-methyl proton (δ_H 2.84 s) to C-1 and C-3, and from H_2-3 to C-1′. Thus, the structure of **2** was defined and named as nicoisoindole A.

The molecular formula of nicoisoindole C (**3**) was determined to be $C_{21}H_{22}N_2O_4$ by the HRMS (ESI) (*m/z* 389.1472 $[M+Na]^+$). The IR spectrum displayed absorptions at 1685 and 1654 cm^{-1} due to carbonyl groups, at 1615, 1582, 1479 cm^{-1} due to aromatic ring. The absorption maxima at 262, 287, and 316 nm observed in UV spectrum due to the aromatic system. Comparison of the 1D NMR (Table 2) and MS spectra of **3** with those of **2** demonstrated that **3** had the same basic skeleton as **2** except for the replacement of the *N*-methyl group in **2** by a 2-(5-methoxy-6-methyl-pyridin-2-yl)ethanamine moiety (C-1′ ~ C-9′, H-3′, H-4′, H_2-7′, H_2-8′, and H_3-9′) in **3**, which was readily supported by the comparisons of NMR data with the similar known compound,

Table 3 Anti-TMV Activity of **1**–**4** on *Nicotiana glutinosa* Leaf[a]

No	% Inhibition at 20 μM	IC_{50} (μM)
1	43.8 ± 3.5	23.6
2	29.6 ± 2.8	46.7
3	58.8 ± 3.6	19.5
4	67.8 ± 3.4	15.4
Ningnanmycin	35.4 ± 3.2	38.0

[a] All results are expressed as mean ± SD; $n = 3$

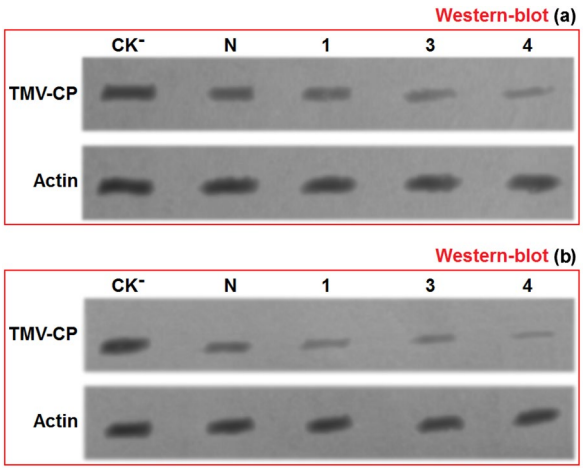

Fig. 4 Western-blot analysis of the accumulation of TMV-CP in the inoculated leaves treated with 20 μM of compounds **1**, **3**, and **4**. [(**a**) on day 3; (**b**) on day 7] (CK.⁻: negative control; N: ningnanmycin; actin serves as the internal reference)

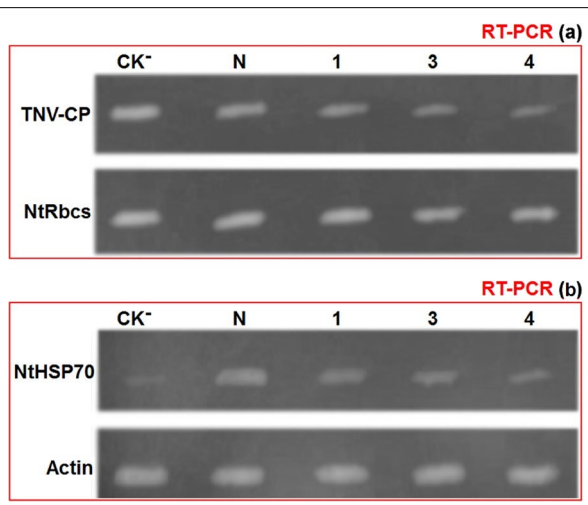

Fig. 5 RT-PCR analyses of the accumulation of TMV-CP in systemic leaves (**a**), and Western-blot analysis of the accumulation of NtHsp70 protein (**b**) in the inoculated leaves. (CK.⁻: negative control; N: ningnanmycin; Mock: healthy tobacco; *NtRbcS* and actin serves as the internal reference)

12′-hydroxy-7′-multijuguinol [28]. The HMBC corrections from H-3′ to C-7′, C-4′ and C-5′, from H-4′ to C-2′, C-3′, and C-6′, from H_2-7′ to C-2′, C-3′, and C-8′, from H_2-8′ to C-7′, from H-9′ to C-5′ and C-6′, and from methoxy proton (δ_H 3.80 s) to C-5′. Moreover, the 2-(5-methoxy-6-methyl-pyridin-2-yl) ethanamine moiety linked to *N*-2 of the isoindolin-1-one nucleus was also established by the HMBC correlations from H_2-8′ to C-1/C-3, and from H_2-3 to C-8′. Therefore, the structure of compound **3** was confirmed, as shown in Fig. 1.

Compound **4** showed a quasi-molecular ion at *m/z* 361.1169 $[M+Na]^+$ in the HRMS (ESI) (calcd. *m/z* 361.1164), corresponding to the molecular formula $C_{19}H_{18}N_2O_4$. The IR spectrum suggested the presence of amine (3368 cm^{-1}), carbonyls (1712, 1683, and 1652 cm^{-1}), and aromatic ring (1612, 1567, and 1465 cm^{-1}), respectively. The UV spectrum showed absorption peaks at 268, 296, and 324 nm suggested the existed of long conjugated system. The ^1H and ^{13}C NMR spectra of **4** were also highly similar to those of **2** in C-1 ~ C-10 and 4-OMe. These indicated that compound **4** is also an isoindolin-1-one skeleton. The main differences were the disappearance *N*-methyl signals and appearance of a *N*-(3-methyl-6-oxo-1,6-dihydropyridin-2-yl) methyl moiety signals (C-2′ ~ C-8′, H-3′, H-4′, H_2-7′, and H_3-8′). These change indicated that the *N*-methyl group in **2** was substituted by a *N*-(3-methyl-6-oxo-1,6-dihydropyridin-2-yl)methyl moiety in **4**. In addition, This deduction was also supported by the comparisons of NMR data with the similar known compound, chrysogedone A [29], and the HMBC corrections from NH-1′ to C-2′/C-3′/C-5′/C-6′/C-7′, from H-3′ to C-2′/C-4′/C-5′, from H-4′ to C-2′/C-6′, from H_2-7′ to C-5′/C-6′, and from H_2-8′ to C-4′/C-5′/C-6′. Furthermore, this substituent at *N*-2 of the isoindolin-1-one nucleus was also confirmed by the HMBC correlations from H_2-7′ to C-1/C-3, and from H_2-3 to C-7′. Thus, the structure of nicoisoindole C (**4**) was established as shown.

Interestingly, compounds **1**–**4** represent a new class of isoindolinone-type small molecule alkaloids with unique cyclopenta[*f*]isoindole-1-one skeletons, and nicoisoindoles C (**3**) and D (**4**) possess rara *N*-2-(5-methoxy-6-methylpyridin-2-yl)ethyl and *N*-(3-methyl-6-oxo-1,6-dihydropyridin-2-yl)methylsubstituents, respectively. Our postulated biosynthetic pathway of the oxocyclopentane moieties in nicoisoindoles A–D is shown in Fig. 3.

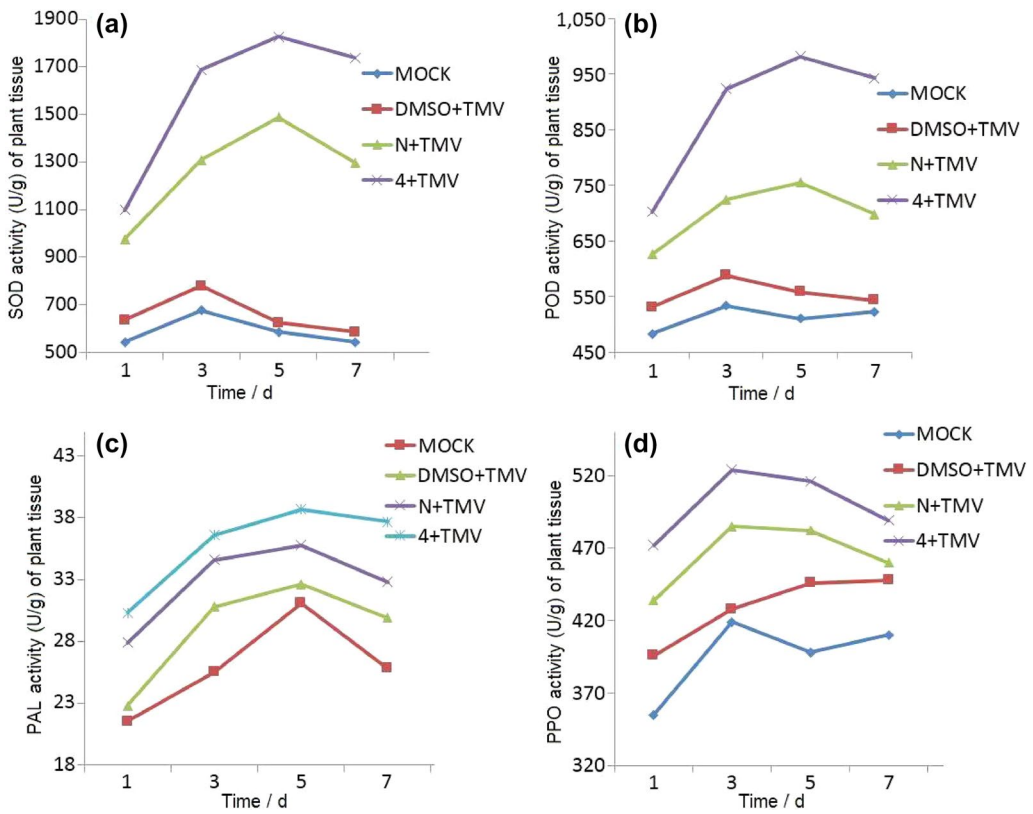

Fig. 6 SOD (**a**), POD (**b**), PAL (**c**), and PPO (**d**) activities in tobacco treated with 20 μM of compound **4**. (Mock: healthy tobacco; N: nignanmycin; all results are expressed as the average value of three determinations for all groups)

The key step was the formation of the oxocyclopentane units by a Friedel-Crafts-like alkylation.

Ant-TMV activities of compounds 1–4

Since many isoindolin-1-one alkaloids from *N. tabacum* have been reported to possess anti-TMV activities [12, 13, 25], nicoisoindoles A–D (**1**–**4**) were evaluated for their anti-TMV activities using the half-leaf method [21, 22]. The results indicated that nicoisoindoles A (**1**), C (**3**) and D (**4**) showed potential anti-TMV activities with inhibition rates of 43.8%, 58.8%, and 67.8% at the concentration of 20 μM (Table 3, Additional file 1: Fig. S29) and with IC_{50} values of 23.6, 19.5, and 15.4 μM, respectively, even more potent than the positive control (ningnanmycin, 35.4% at 20 μM and IC_{50} value of 38.0 μM). Furthermore, nicoisoindoles C (**3**) and D (**4**) also exhibited protective effects to the host plants with the inhibition rates 52.8 ± 4.2% and 62.6 ± 4.0% (Additional file 1: Fig. S30), respectively. These results may suggest that pretreatment with nicoisoindoles C (**3**) and D (**4**) enhance the resistance of the host plant against TMV infection.

The induction of SAR in the tobacco for compounds 1, 3 and 4

To assess whether the protective effects of compounds **1**, **3** and **4** were due to the induction of systemic acquired resistance (SAR) in the tobacco plants, the SAR for these three compounds was screened against in the systemically infected host *N. tabacum* cv. HD, and conducted western bolt analysis of tobacco mosaic virus capsid protein (TMV-CP) (Fig. 4). In Fig. 4a, the bands intensities of TMV-CP indicated that on day 3 after inoculation, the accumulation of TMV-CP in the leaves treated with compounds **1**, **3** and **4** were significantly less than that of in the negative control. In addition, the accumulations were also obvious less than that of ningnanmycin, and compound **4** has the lowest band. The results are agreed with the inhibition rates obtained from half-leaf method. In Fig. 4b (on day 7 after inoculation), the trends for bands intensities of TMV-CP are agreed with these on day 7. However, the bands intensities of **1**, **3** and **4** were obvious less than these on day 7. The results revealed that **1**, **3** and **4** have the protective effects due to the induction of SAR.

Furthermore, the anti-TMV efficiencies of compounds **1**, **3** and **4** on day 7 were further confirmed by semi-quantitative RT-PCR assay at the transcription level of 20 μM, based on the results of the western blot assay of TMV-CP. The newly grown leaves of *N. tabacum* cv. HD on day 7 was used as the RT-PCR assay material. The results (Fig. 5a) revealed that the transcription levels of TMV-CP in the newly grown leaves of the plants were noticeably less than that of in the treatment group of the negative control. The results are corroborated with that of western-blot analysis. According to the above observations, compound **1**, **3**, and **4** may exhibited anti-TMV activities through the inhibition of accumulation of the TMV-CP protein, and the systemic leaves showed a relatively higher induction.

The effect of compound 4 on defense-related enzyme activities

Since the activities enzymes involved in plant defense resistance (PAL, POD, SOD, PPO, and the like) are significantly related to plant defense [23, 30], the activities enzymes were also analyzed in 20 μM compound

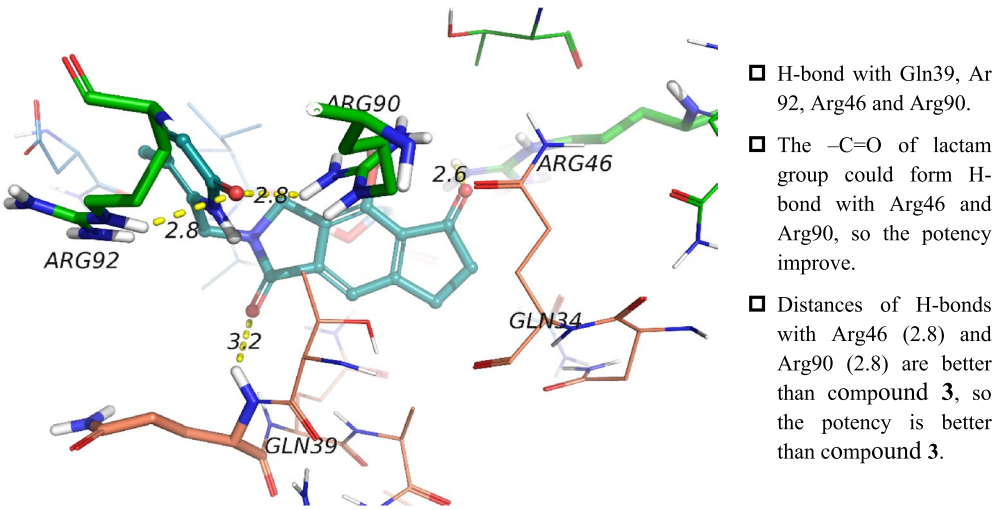

Fig. 7 Interactions of compound **4** and TMV-helicase (key residues are represented as sticks and H-bonds are represented by solid lines)

Table 4 Anti-rotavirus activity of compounds **1**–**4**

No	CC_{50} (μg/mL)	EC_{50} (μg/mL)	TI (CC_{50}/EC_{50})
1	172.2	13.2	13.0
2	247.2	14.4	17.2
3	206.4	13.2	15.6
4	218.5	11.8	18.5
Ribavirin	258.4	12.2	21.2

CC_{50}: mean (50%) value of cytotoxic concentration; EC_{50}: mean (50%) value of effective concentration

TI therapeutic index, CC_{50}/EC_{50}

4 treated tobacco leaves, and the results are shown in Fig. 6. The results are revealed that the POD activities of the DMSO + TMV, ningnanmycin + TMV, and **4** + TMV treatment groups were higher than that of mock group. Notably, the SOD (Fig. 6a) and POD (Fig. 6b) activities of **4** + TMV treatment group have significantly increases. However, the increases of PAL (Fig. 6c) and PPO (Fig. 6d) activities have not so significant. The POD and SOD activities reach the maximum on day 5, and then the activities decreases. On day 5, the SOD of **4** + TMV treatment group is 3.12 fold higher than that of the MOCK group, 2.93 fold higher than that of DMSO + TMV group, and 1.23 fold higher than that of ningnanmycin + TMV group, the POD of **4** + TMV treatment group is 1.93 fold higher than that of the MOCK group, 1.76 fold higher than that of DMSO + TMV group, and 1.30 fold higher than that of ningnanmycin + TMV group. POD and SOD are oxidoreductive enzymes and are involved in cell wall biosynthesis. The ROS generation can protects plant cells from ROS-induced oxidative damage, reflect the state of photosynthesis, and enhance tobacco resistance to TMV. Therefore, this induction defensive responses maybe improve disease TMV resistance. POD is associated with plant defense and can induce the biosynthetic pathway of salicylic acid (SA), lignin, and phytoalexins, it can activate SAR and pathogen inhibition, and can promote cell-wall reinforcement. The results presented in this paper indicate that the activities of POD and SOD are significantly up-regulated in the TMV-infected plants with compound **4** pre-treatment, and this induce maybe the reason for improving the TMV resistance of tobacco.

The effect of compounds 1, 3 and 4 on NtHsp70 protein expression

In addition to the activities enzymes, the expression of Hsp70 can influence virus infection in plants by promoting viral accumulation and movement [31]. In tobacco, the expression of NtHsp70 gene is also closely related to the tobacco plants resistance to TMV [32]. Therefore, In this study, the NtHsp70 expression was also analyzed on day 7 when TMV was inoculated 12 h after foliar spraying with 20 μM of compound **1**, **3** and **4**. The expression of total NtHsp70 protein in TMV-inoculated tobacco and different compound-treated groups was higher than that in healthy tobacco leaves (Fig. 5b), and the total NtHsp70 protein accumulation were significant reduced in groups treated with **1**, **3** and **4**. This result is as same as that of compounds **1**, **3** and **4** in reducing TMV-CP accumulation. This down-regulate was also suggested compounds **1**, **3** and **4** associated inhibition of TMV infection through the suppressing NtHsp70 expression.

The molecular docking analysis between antiviral agents and TMV-Hel

In this study, compounds **1–4** showed potential anti-TMV activities. To screen the inhibitors based on TMV-Hel structure, we performed molecular docking experiment. The 2 TMV-Hel crystal protein structures were released in the RSCB PDB database, and we chose the crystal structure (PDB: 2OM3) resolved by literature [33] with better resolution as the receptor, and the small molecules in the crystal structure as the control substrate. The docking results are shown in Fig. 7 and Additional file 1: Figs. S31–S33, and Additional file 1: Table S1. Compounds 1–4 showed similar docking scores to the original ligand in the crystal structure, indicating that compounds 1–4 have similar protein binding with the original ligand. For compound **1**, the H-bond is affinitized with Gln39 and Arg46, and the -NH of lactam may also can form a water bridge with Arg92. The red circle space is not occupied by small molecules, and this region is highly polarized, so water will occupy the pocket. Thus, the water bridge interaction is formed between ligand and protein. Therefore, this compound has potency. For compound **2**, H-bond is affinitized with Arg92 and Arg46, and it lost the water bridge with Arg92, so the potency drops. *N*-methyl only form Hydrophobic interactions with protein, and will replace waters, so lost water bridge interaction. This also cause the potency drops. For compound **3**, H-bond is affinitized with Gln39, Arg92, Arg90 and Arg46, the *N*-atom of pyridine group also can form H-bond with Arg46 and Arg90, so the potency notably improve. For compound **4**, H-bond is affinitized with Gln39, Arg92, Arg46 and Arg90, the − C=O of lactam group also can form H-bond with Arg46 and Arg90, so the potency significantly improve. In addition, the distances of H-bonds with Arg46 (2.8) and Arg90 (2.8) are better than compound **3**, so the potency is better than compound **3**. These docking results were consistent with the in vitro anti-TMV experiment. Which may revealed that the oxocyclopenta[*f*]isoindole-1-one nucleus of compounds **1–4** is fundamental for anti-TMV activities. The 2-(5-methoxy-6-methyl-pyridin-2-yl)ethanamine moiety

in **3**, and *N*-(3-methyl-6-oxo-1,6-dihydropyridin-2-yl) methylmoiety in **4** at *N*-2 position may increases the inhibitory activities. These studies of structure–activity relationship are helpful to find new anti-TMV activities inhibitors.

Anti-rotavirus activities of compounds 1–4

To study whether the oxocyclopenta[*f*]isoindoles has more broad antiviral activities, compounds **1**–**4** were also tested for their anti-rotavirus activity. Their ability to prevent the cytopathic effects of rotavirus in MA104 cells was tested according to our previous literatures [32], and their effects were measured in parallel with the determination of antiviral activities using ribavirin as positive control. The results (Table 4) revealed that compounds **1**–**4** exhibited potential anti-rotavirus activities with therapeutic index (TI) in the range of 13.0–18.5.

Conclusions

In this study, nicoisoindoles A–D, four new isoindolinone alkaloids with cyclopenta[*f*]isoindole-1-one frameworks, were obtained from the stems of tobacco. Interestingly, compounds **1**, **3** and **4** showed high anti-TMV activities with inhibition rates of 43.8%, 58.8%, and 67.8%, and IC_{50} values of 23.6, 19.5 and 15.4 μM, respectively, even more potent than ningnanmycin. In additions, compounds **1**–**4** were also exhibited potential anti-rotavirus activity with therapeutic index (TI) valves in the range of 13.0–18.5. This also indicated that the new compounds have more broad antiviral activities. The successful isolation and structure identification of oxocyclopenta[*f*] isoindole-1-ones provide materials for the screening of antivirus activities inhibitors, and also contribute to the development and utilization of the waste from tobacco cultivation.

Supplementary Information

The online version contains supplementary material available at https://doi.org/10.1186/s40538-022-00339-7.

Additional file 1: Figure S1. 13C and DEPT NMR spectrum tobindole A (1). **Figure S2.** ^{1}H NMR spectrum of tobindole A (1). **Figure S3.** HSQC NMR spectrum of tobindole A (1). **Figure S4.** HMBC NMR spectrum of tobindole A (1). **Figure S5.** HRMS spectrum of tobindole A (1). **Figure S6.** UV spectrum of tobindole A (1). **Figure S7.** IR spectrum of tobindole A (1). **Figure S8.** ^{13}C and DEPT NMR spectrum tobindole B (2). **Figure S9.** ^{1}H NMR spectrum of tobindole B (2). **Figure S10.** HSQC NMR spectrum of tobindole B (2). **Figure S11.** HMBC NMR spectrum of tobindole B (2). **Figure S12.** HRMS spectrum of tobindole B (2). **Figure S13.** UV spectrum of tobindole B (2). **Figure S14.** IR spectrum of tobindole B (2). **Figure S15.** ^{13}C and DEPT NMR spectrum tobindole C (3). **Figure S16.** ^{1}H NMR spectrum of tobindole C (3). **Figure S17.** HSQC NMR spectrum of tobindole C (3). **Figure S18.** HMBC NMR spectrum of tobindole C (3). **Figure S19.** HRMS spectrum of tobindole C (3). **Figure S20.** UV spectrum of tobindole C (3). **Figure S21.** IR spectrum of tobindole C (3). **Figure S22.** ^{13}C and DEPT NMR spectrum tobindole D (4). **Figure S23.** ^{1}H NMR spectrum of tobindole D (4). **Figure S24.** HSQC NMR spectrum of tobindole D (4). **Figure S25.** HMBC NMR spectrum of tobindole D (4). **Figure S26.** HRMS spectrum of tobindole D (4). **Figure S27.** UV spectrum of tobindole D (4). **Figure S28.** IR spectrum of tobindole D (4). **Figure S29.** The antiviral inhibition rates tested by half-leaf method for ningnanmycin, compounds 1, 3 and 4. **Figure S30.** The protective effects of compounds 3 and 4 on TMV. **Figure S31.** Interactions of 1 and TMV-helicase. **Figure S32.** Interactions of 2 and TMV-helicase. **Figure S33.** Interactions of 3 and TMV-helicase. **Figure S34.** Polymers and ligands' pocket of TMV-helicase. **Table S1.** Docking score of compounds 1-4 and original ligand in the TMV-Hel structure.

Acknowledgements

We appreciate the Kunming Institute of Botany, Chinese Academic Sciences, for use of the Schrodinger Suite software.

Author contributions

QH, MZ, XL, and GY designed the experiment. JZ, JW, and XL prepared the samples, QH, YM, HL, JD, FY, JL, WW, MZ, and GY performed the experiments, analysed data and wrote the paper. QH, YL, MZ, and GY reviewed and checked all the details. All authors read and approved the final manuscript.

Funding

This work was supported financially by the Foundation of Yunnan basic research program (No. 2019FD086), the National Natural Science Foundation of China (No. 21967021 and No. 21762050), the Foundation of Yunnan Tobacco Industry Co. Ltd (No. 2021JC08), the Foundation of China Tobacco Company [No. 110202101004 (JY-04)], the Yunnan Applied Basic Research Projects for Excellent Young Scholars (No. 202001AW070002).

Availability of data and materials

The following supplementary materials can be downloaded at: https:

Declarations

Ethics approval and consent to participate

Not applicable.

Consent for publication

This research has been confirmed for publication in the journal.

Competing interests

The authors have no conflicts of interest.

Received: 20 July 2022 Accepted: 17 September 2022
Published online: 16 November 2022

References

1. Vagg R, Chapman S. Nicotine analogues: a review of tobacco industry research interests. Addiction. 2015;100:701–12. https://doi.org/10.1111/j.1360-0443.2005.01014.x.
2. Jassbi AR, Zare S, Asadollahi M, Schuman MC. Ecological roles and biological activities of specialized metabolites from the genus *Nicotiana*. Chem Rev. 2017;117:12227–80. https://doi.org/10.1021/acs.chemrev.7b00001.
3. He XF, Hou XD, Ren X, Guo K, Li XZ, Yan ZQ, Du YM, Zhang ZF, Qin B. Two new cembranic diterpenoids from the flowers of *Nicotiana tabacum* L. Phytochem Lett. 2016;15:238–44. https://doi.org/10.1016/j.phytol.2016.02.006.
4. Becerra-Martinez E, Pacheco-Hernandez Y, Lozoya-Gloria E, Betancourt-Jimenez MG, Hidalgo-Martinez D, Zepeda-Vallejo LG, Villa-Ruano N. ^{1}H-NMR metabolomics profiling of recombinant tobacco plants holding a promoter of a sesquiterpene cyclase. Phytochem Anal. 2020;31:480–7. https://doi.org/10.1002/pca.2911.
5. Shen QP, Xu XM, Li L, Zhao W, Xiang NJ, Yang GY, Chen YK, Miao MM, Liu CB, Liu ZH. Sesquiterpenes from the leaves of *Nicotiana tabacum* and

their anti-tobacco mosaic virus activity. Chin Chem Lett. 2016;27:753–6. https://doi.org/10.1016/j.cclet.2016.01.048.
6. Shang SZ, Shi JL, Tang JG, Jiang JX, Zhao W, Zheng XD, Lei P, Han JM, Wang CY, Yuan DL, Yang GY, Chen YK, Miao MM. New isolates from leaves of *Nicotiana tabacum* and their biological activities. Nat Prod Res. 2019;33:1577–83. https://doi.org/10.1080/14786419.20181425840.
7. Chien SK, Chen LC, Huang HC, Chen LC, Hsiao JW, Cheng MJ, Chen JJ. A new flavone and cytotoxic constituents of *Nicotiana tabacum*. Chem Nat Compds. 2018;54:1044–7. https://doi.org/10.1007/s10600-018-2551-4.
8. Hu QF, Luo D, Lv N, Li YK, Kong WS, Li J, Liu X, Gao Q, Yang GY, Xiang HY, Jiang JX. Pentenyl coumarins from the roots and stems of Yunnan local sun cured tobacco and their bioactivity. Heterocycles. 2019;98:1747–54. https://doi.org/10.3987/COM-19-14188.
9. Zhu LJ, Luo D, Lv N, Li YK, Mi QL, Wang J, Kong WS, Gao Q, Li GP, Yang GY, Hu QF, Guan Y, Ye YQ. Two new coumarins from the roots and stems of *Nicotiana tabacum* and their bioactivity. Chem Nat Compds. 2020;56:806–10. https://doi.org/10.1007/s10600-020-03157-1.
10. Li YK, Lv N, Luo D, Kong WS, Mi QL, Gao Q, Zeng WL, Li J, Ling J, Liu CB, Yang GY, Li XM, Chen ZY, Hu QF. Three new furan-2-carboxylic acid derivatives from the stem bark of *Nicotiana tabacum* and their bioactivity. Heterocycles. 2020;100:267–75. https://doi.org/10.3987/COM-19-14198.
11. Wang X, Huang LJ, Liang MJ, Li YK, Zeng WL, Xiang HY, Li J, Liu X, Mi QL, Guo YD, Yang GY, Deng L, Gao Q. Two new furan-2-carboxylic derivatives from the leaves of *Nicotiana tabacum* and their anti-tobacco mosaic virus activities. Chem Nat Compds. 2020;56:848–51. https://doi.org/10.1007/s10600-020-03167-z.
12. Zhang JD, Liu X, Xu L, Jiang JR, Deng LL, Yang WW, Li XM, Yang GY, Zhou T, Yang FX. Anti-tobacco mosaic virus isoindolin-1-ones from the stems of *Nicotiana tabacum*. Heterocycles. 2021;102:1167–74. https://doi.org/10.3987/COM-21-14435.
13. Kong GH, Wu YP, Li W, Xia ZY, Liu Q, Wang KM, He P, Zhu RZ, Si XX, Yang GY. Two new isoindolin-1-ones from the leaves of *Nicotiana tabacum* and their anti-tobacco mosaic virus activities. Heterocycles. 2016;92:331–6. https://doi.org/10.3987/COM-15-13331.
14. Yildiz D. Nicotine its metabolism and an overview of its biological effects. Toxicon. 2004;43:619–32. https://doi.org/10.1016/j.toxicon.2004.01.017.
15. Wahlberg I, Enzell CR. Tobacco isoprenoids. Nat Prod Rep. 1987;4:237–76. https://doi.org/10.1039/NP9870400237.
16. Loughrin JH, Hamilton-Kemp TR, Andersen RA, Hildebrand DF. Headspace compounds from flowers of *Nicotiana tabacum* and related species. J Agric Food Chem. 1990;38:455–60. https://doi.org/10.1021/jf00092a027.
17. Khan S, Pandey SS, Jyotshna Shanker K, Rahman LU. Cloning and functional characterization of quinolinic acid phosphoribosyl transferase QPT gene of *Nicotiana tabacum*. Physiol Plant. 2017;160:253–65. https://doi.org/10.1111/ppl.12559.
18. Tang ZX, Chen LL, Chen ZB, Fu YL, Sun X, Wang BB, Xia TY. Climatic factors determine the yield and quality of Honghe flue-cured tobacco. Sci Rep. 2020;10:868. https://doi.org/10.1038/s41598-020-76919-0.
19. Sharma A, Singh Y, Singh NK, Singla A, Chen WH. Effective utilization of tobacco *Nicotiana tabaccum* for biodiesel production and its application on diesel engine using response surface methodology approach. Fuel. 2020;273: 117793. https://doi.org/10.1016/j.fuel.2020.117793.
20. Qin ZD, Sun MX, Luo XF, Zhang HR, Xie JY, Chen HF, Yang LR, Shi L. Life-cycle assessment of tobacco stalk utilization. Bioresour Technol. 2018;265:119–27. https://doi.org/10.1016/j.biortech.2018.05.110.
21. Hu QF, Zhou B, Huang JM, Gao XM, Shu LD, Yang GY, Che CT. Antiviral phenolic compounds from *Arundina gramnifolia*. J Nat Prod. 2013;76:92–296. https://doi.org/10.1021/np300727f.
22. Zhou M, Zhou K, Gao XM, Jiang ZY, Lv JJ, Liu ZH, Yang GY, Miao MM, Che CT, Hu QF. Fistulains A and B New bischromones from the bark of *Cassia fistula* and their activities. Org Lett. 2015;17:2638–41. https://doi.org/10.1021/acs.orglett.5b01007.
23. Yan Y, Wang D, Zhang X, Peng MY, Yan XY, Guo YS, Jia MG, Zhou J, Tang L, Hao XJ. Anti-TMV activity and effects of three prieurianin-type limonoids from *Munronia henryi*. Pestic Biochem Physiol. 2022;184: 105108. https://doi.org/10.1016/j.pestbp.2022.105108.
24. Hu QF, Wu F, Zhou T, Zhou M, Zhu YN, Cai BB, Liu MX, Li MF, Yang GY, Li YK. Three new anti-rotavirus chromeno[3,2-*c*]pyridines from the whole plant of *Thalictrum scabrifolium*. Heterocycles. 2021;102:1810–6. https://doi.org/10.3987/COM-21-14505.
25. Zhang FM, Xia JJ, Yang PS, Shen QP, Liu CB, He P, Wang JQ, Liu ZH, Ding ZT. Three new isoindolin-1-ones from the leaves of Yunnan local sun cured tobacco and their bioactivities. Heterocycles. 2016;92:1713–20. https://doi.org/10.1002/chin.201652427.
26. Beukes DR, Davies-Coleman MT, Kelly-Borges M, Harper MK, Faulkner DJ. Dilemmaones A—C unusual indole alkaloids from a mixed collection of South African sponges. J Nat Prod. 1998;61:699–701. https://doi.org/10.1021/np970580m.
27. Lambson KE, Dacko CA, Mcneill JM, Akhmedov NG, Sderberg B. Synthesis of the tricyclic indole alkaloids dilemmaones A and B. Tetrahedron. 2019;75: 130714. https://doi.org/10.1016/j.tet.2019.130714.
28. Welington F, Marcos P, Amanda D, Luis OR, Luciene RB, Maria CMY, Norberto PL, Joao LCL, Vanderlan SB. Pyridine alkaloids from *Senna multijuga* as acetylcholinesterase inhibitors. J Nat Prod. 2012;75:408–13. https://doi.org/10.1021/np200814j.
29. Peng XP, Wang Y, Sun KL, Liu PP, Yin X, Zhu WM. Cerebrosides and 2-pyridone alkaloids from the Halotolerant fungus *Penicillium chrysogenum* grown in a hypersaline medium. J Nat Prod. 2011;74:1298–302. https://doi.org/10.1021/np1008976.
30. Dietz KJ, Turkan I, Krieger-Liszkay A. Redox-and reactive oxygen species-dependent signaling into and out of the photosynthesizing chloroplast. Plant Physiol. 2016;171:1541–50. https://doi.org/10.1104/pp.16.00375.
31. Kanzaki H, Saitoh H, Ito A, Fujisawa S, Kamoun S, Katou S, Yoshioka H, Terauchi R. Cytosolic Hsp90 and Hsp70 are essential components of INF1-mediated hypersensitive response and non-host resistance to *Pseudomonas cichorii* in *Nicotiana benthamiana*. Mol Plant Pathol. 2003;4(5):383–91. https://doi.org/10.1046/j.1364-3703.2003.00186.x.
32. Song ZP, Pan FL, Lou XP, Wang DB, Yang C, Zhang BQ, Zhang HY. Genome-wide identification and characterization of hsp70 gene family in *Nicotiana tabacum*. Mol Biol Rep. 2019;46:1941–54. https://doi.org/10.1007/s11033-019-04644-7.
33. Sachse C, Chen JZ, Coureux PD, Stroupe ME, Fandrich M, Grigorieff N. High resolution electron microscopy of helical specimens a fresh look at tobacco mosaic virus. J Mol Biol. 2007;371(3):812–35. https://doi.org/10.1016/j.jmb.2007.05.088.

Publisher's Note